Regional difference in the distribution of alkaline phosphatase, PHOSPHO1, and calcein labeling in the femoral metaphyseal trabeculae in parathyroid hormone-administered mice

Mai Haraguchi-Kitakamae[1,2], Yuhi Nakajima[3], Tomomaya Yamamoto[2,4], Hiromi Hongo[2], Jiaxin Cui[2], Yan Shi[2], Xuanyu Liu[2,5], Qi Yao[2], Haruhi Maruoka[2], Miki Abe[2], Tamaki Sekiguchi[5], Ayako Yokoyama[6], Norio Amizuka[2], Yasuyuki Sasano[1], and Tomoka Hasegawa[2§]

[1]Division of Craniofacial Development and Tissue Biology, Graduate School of Dentistry, Tohoku University, Sendai, Japan, [2]Ultrastructure of Hard Tissue, Graduate School of Dental Medicine, Faculty of Dental Medicine, Hokkaido University, Japan, [3]Department of Oral and Maxillofacial Surgery, Nagoya University Hospital, Nagoya, Japan, [4]Department of Dentistry, Japan Ground Self-Defense Force, Camp Shinmachi, Japan, [5]Oral and Maxillofacial Surgery, Graduate School of Dental Medicine, Faculty of Dental Medicine, Hokkaido University, Japan, [6]Gerodontology, Graduate School of Dental Medicine, Faculty of Dental Medicine, Hokkaido University, Japan.

Running Headline/Short Title: Regional difference in PTH anabolism in bone

[§]**Address for correspondence:**

Tomoka Hasegawa, DDS, Ph.D.

Ultrastructure of Hard Tissue, Faculty of Dental Medicine, Hokkaido University, Japan,

Phone/Fax: +81-11-706-4226

E-mail: hasegawa@den.hokudai.ac.jp

Abstract

Objectives: This study aimed to elucidate whether the administration of parathyroid hormone (PTH) results in remodeling- or modeling-based bone formation in different regions of the murine femora, and whether the PTH-driven bone formation would facilitate osteoblastic differentiation into osteocytes.

Methods: Six-week-old male C57BL/6J mice were employed to examine the distribution of alkaline phosphatase (ALP), PHOSPHO1, podoplanin, and calcein labeling in two distinct long bone regions: the metaphyseal trabeculae close to the chondro-osseous junction (COJ) and those distant from the COJ in three mouse groups, a control group receiving a vehicle (Sham group) and groups receiving hPTH (1-34) twice a day (PTH BID group) or four times a day (PTH QID group) for two weeks.

Results: The Sham group showed PHOSPHO1-reactive mature osteoblasts localized primarily at the COJ, whereas the PTH BID/QID groups exhibited extended lines of PHOSPHO1-reactive osteoblasts even in regions distant from the COJ. The PTH QID group displayed fragmented calcein labeling in trabeculae close to the COJ, whereas continuous labeling was observed in trabeculae distant from the COJ. Osteoblasts tended to express podoplanin and PHOSPHO1 independently in the close and distant regions of the Sham group, while osteoblasts in the PTH-administered groups showed immunoreactivity of podoplanin and PHOSPHO1 together in the close and distant regions.

Conclusions: Administration of PTH may accelerate remodeling-based bone formation in regions close to the COJ while predominantly inducing modeling-based bone formation in distant regions. PTH

appeared to simultaneously facilitate osteoblastic bone mineralization and differentiation into osteocytes in both remodeling- and modeling-based bone formation.

Keywords: bone tissue**,** parathyroid hormone, alkaline phosphatase, PHOSPHO1, immunohistochemistry

1. Introduction

Parathyroid hormone (PTH) stimulates both bone formation and bone resorption, ultimately resulting in anabolic effects on the bone [1-4]. The current understanding of bone formation induced by osteoporotic drugs can be categorized into two primary histological processes: remodeling and modeling-based bone formation [5]. The anabolic effects of teriparatide are believed to be primarily attributable to an enlarged anabolic window during accelerated remodeling-based bone formation [6]. In contrast, bone modeling involves changes in bone size and shape, and is independent of osteoclastic activity, suggesting the uncoupling of bone formation and resorption [7-10]. Osteoporotic drugs such as the anti-human sclerostin antibody romosozumab efficiently induce modeling-based bone formation, promoting bone formation without being accompanied by bone resorption [11-13]. Therefore, teriparatide and romosozumab are classified as osteoporotic drugs, leading to remodeling-based and model-based bone formation, respectively.

Nevertheless, we have previously reported that frequent PTH administration results in remodeling-based bone formation, characterized by numerous thin trabeculae surrounded by thick layers of preosteoblastic cells containing several osteoclasts [14]. Conversely, low-frequency PTH administration induces remodeling and modeling-based bone formation with relatively thick trabeculae. Therefore, the frequency of PTH administration may influence the mode of bone formation, *i.e.,* whether it follows remodeling- or modeling-based bone formation [14]. We also considered that different regions of the metaphyses in the long bones might exhibit distinct anabolic effects in PTH-

administered mice. Thus, it is essential to investigate whether different modes of bone formation occur in various regions of PTH-administered bones.

Additionally, we investigated whether the speed of osteoblast differentiation into osteocytes was affected by PTH-driven bone formation. Our recent findings indicate that matrix synthesis and bone mineralization are enhanced in PTH-administered bones [15]. However, we investigated whether osteoblasts could simultaneously mineralize the bone matrix and differentiate into osteocytes under normal conditions and in a PTH-induced anabolic environment. Therefore, it is important not only to determine whether PTH administration results in remodeling-based or modeling-based bone formation in different regions but also to elucidate whether the timing of osteocytic differentiation from bone-mineralizing osteoblasts changes in regions with PTH-driven remodeling-based or modeling-based bone formation.

Histological and histomorphometric assessments are necessary to clarify these issues. Regarding histological markers of anabolic activity, tissue nonspecific alkaline phosphatase (ALP, an enzyme that synthesizes monophosphate ions), phosphoethanolamine/phosphocholine phosphatase 1 (PHOSPHO1, an enzyme that hydrolyzes phosphocholine and phosphoethanolamine to release phosphate ions within matrix vesicles), and calcein labeling are commonly used to evaluate anabolic effects in bone histomorphometric analyses. ALP is widely distributed in preosteoblastic cells and mature osteoblasts [16, 17], whereas PHOSPHO1 appears to be specifically expressed in mature osteoblasts involved in matrix vesicle synthesis, *i.e.,* bone-mineralizing osteoblasts [18, 19]. Calcein labeling is typically

employed to visualize mineral deposition in bone [20]. Therefore, ALP is suitable for illustrating the broad distribution of osteoblastic cells, whereas PHOSPHO1 and calcein labeling are indicators of mineralizing mature osteoblasts and mineral deposition, respectively. Podoplanin is reportedly expressed during the early stages of osteocytes [21, 22]. As in previous reports [23-25], we observed podoplanin expression in osteoblasts that were bound to differentiate into osteocytes and/or osteocytes embedded in the bone [26]. Therefore, podoplanin appears to be a suitable marker for osteoblast differentiation into osteocytes and newly differentiated osteocytes.

Thus, our study aimed to examine whether intermittent PTH administration induces remodeling- or modeling-based bone formation in various regions of long bones and whether it alters the timing of osteocytic differentiation from bone-mineralizing osteoblasts via histochemical assessment techniques.

2. Materials and Methods

2.1. Animals

Six-week-old male C57BL/6J mice (n = 18; Japan CLEA, Tokyo, Japan) were handled in accordance with Hokkaido University's guidelines for animal care and research use (approved protocol #20-0019). Mice were allocated to a control group that received vehicle only (sham group, 0.9% saline, n=6) or a PTH group that received hPTH (1-34) (Sigma-Aldrich Co., LLC., St. Louis, MO, n=12). As previously described [14], mice received 20 μg/kg/day of hPTH (1-34) two times per day (PTH BID group, bis

in die, n = 6) or four times per day (PTH QID group, quater in die, n = 6) for 2 weeks.

2.2. Specimen preparation

For bone labeling, the mice were injected subcutaneously with 20 mg/kg of 0.1% calcein solution 3 and 6 days before sacrifice. They were fixed with 4% paraformaldehyde in 0.1 M phosphate buffer (pH 7.4) through the left ventricle under anesthesia with an intraperitoneal injection of a combination of anesthetic agents prepared with 0.3 mg/kg of medetomidine, 4.0 mg/kg of midazolam, and 5.0 mg/kg of butorphanol. The femora were removed and immediately immersed in the same fixative for 24 h. The left femora were decalcified with 10% ethylenediaminetetraacetic disodium salt for 2 months at 4 °C before paraffin embedding. Five μm-thick sagittal sections were cut parallel to the bone longitudinal axis. To detect calcein labeling, the right femora was immersed in 70% ethanol after perfusion for 18 h before being embedded in methyl methacrylate. All sections subjected to histochemical staining were photographed using a Nikon Eclipse E800 microscope (Nikon Instruments Inc., Tokyo, Japan) and images were acquired using a digital camera (Nikon DXM1200C, Nikon).

2.3. Immunohistochemistry for ALP, PHOSPHO1, and podoplanin

Dewaxed paraffin sections were examined for ALP, PHOSPHO1, and podoplanin as previously reported [15, 16]. The sections were immersed in 0.3% H_2O_2 in phosphate-buffered saline (PBS) for 30 min to block endogenous peroxidase, and 1% bovine serum albumin (Serologicals Proteins Inc.,

Kankakee, IL) in PBS was applied to the sections for 20 min to reduce nonspecific binding. The sections were incubated with primary and secondary antibodies. The antibiotics used are listed in supplementary table 1. After incubation with antibodies, diaminobenzidine tetrahydrochloride (DAB) was used as a substrate to visualize all horseradish peroxidase (HRP)-conjugated immunoreactions. All the sections were counterstained with methyl green.

2.4. Double detection of podoplanin and PHOSPHO1

For double detection of podoplanin and PHOSPHO1, the sections were treated with a polyclonal podoplanin antibody and subsequent HRP-conjugated rabbit anti-goat IgG for DAB visualization. Sections were then incubated with rabbit polyclonal anti-PHOSPHO1 antibody, followed by ALP-conjugated goat anti-rabbit IgG. ALP histochemistry was performed as previously described [3]; in short, the sections were incubated in a mixture of 2.5 mg of naphthol AS-BI phosphate (Sigma-Aldrich), 18 mg of fast blue BB salt (Sigma-Aldrich) diluted in 30 ml of a 0.1 M Tris-HCl buffer (pH 8.5) for 15 min at 37 °C.

2.5. Enzyme histochemistry for tartrate-resistant acid phosphatase

Tartrate-resistant acid phosphatase (TRAP) was detected as previously described [27]; dewaxed paraffin sections were rinsed with PBS and incubated in a mixture of 2.5 mg of naphthol AS-BI phosphate, 18 mg of red violet LB salt (Sigma-Aldrich), and 100 mM L(+) tartaric acid (0.76 g, Nacalai

Tesque, Inc., Kyoto, Japan) diluted in 30 ml of a 0.1 M sodium acetate buffer (pH 5.0) for 15 min at 37 °C.

2.6. Selection of the different regions of interest in metaphyses

We previously examined a 600 m × 600 m area located just below the growth plate of the femoral metaphysis [28]. However, we divided this area into two in this study - assumed boxed areas (the region of interest: ROI) with 600 μm (width) × 300 μm (length) located just below the bottom of the femoral COJ (the region close to the COJ), and 600 μm (width) × 300 μm (length) with 330 μm distant from the bottom of the femoral COJ (the region distant from the COJ).

2.7. Quantification of bone histomorphometric parameters and immunohistochemistry

In two different regions (ROIs) close to and distant from the COJ, bone volume/tissue volume (BV/TV), trabecular number (Th.N), and trabecular thickness (Tb.Th.), ALP-positive area/TV, PHOSPHO1-positive area/TV, bone formation rate/bone surface (BFR/BS), the average length of calcein labeling, osteoclast numbers/tissue volume (Oc.N/TV), osteoclast numbers/BS (Oc.N/BS), podoplanin-positive area/TV, and the ratio of osteoblasts positive for both PHOSPHO1 and podoplanin were examined using Image-Pro Plus 6.2 (Media Cybernetics, Inc., Bethesda MD) as reported by Yamamoto et al. [14]. Whenever possible, abbreviations and calculations followed the recommendations of the ASBMR Histomorphometry Nomenclature Committee [29]. Similar to the ratio of osteoblasts positive for

PHOSPHO1 and podoplanin, we recognized osteoblasts bearing podoplanin immunoreactivity, excluding those embedded or fully embedded in the bone matrix, as podoplanin-positive osteoblasts. We counted the number of PHOSPHO1-reactive and podoplanin-positive osteoblasts and divided them by the total number of osteoblasts. BFR and average calcein labeling length were assessed according to our previous report [14]. TRAP-positive cells with more than two nuclei were considered multinucleated osteoclasts. The osteoclast numbers/BS ratio indicated the number of osteoclasts localized on the bone surfaces and excluded osteoclasts that were not on the bone surfaces.

2.8. Statistical analysis

All statistical analyses were assessed by one-way ANOVA followed by the Tukey-Kramer multiple comparisons test, with all values presented as mean ± SD. Statistical significance was set at $P < 0.05$ were considered significant.

3. Results

3.1. Histological analysis of metaphyseal trabeculae

Two distinct ROIs close to and distant from the COJ were applied to both the sham and PTH BID/QID groups (**Figures 1A-C**). The PTH-treated groups (**Fig. 1B, C**) exhibited more metaphyseal trabeculae than the sham group **(Fig. 1A)**. Notably, the PTH group displayed thicker trabeculae in the region

distant from the COJ than the sham group **(Figure 1D)**. The PTH group demonstrated a higher BV/TV value in the region close to the COJ than the Sham group **(Fig. 1G)**. The PTH QID group exhibited the highest Tb.N **(Fig. 1H)**, whereas the PTH BID group showed significantly elevated Tb.Th **(Fig. 1I)**. In contrast, in the region distant from the COJ, the PTH QID group displayed increased BV/TV and Tb.N compared with the PTH BID group **(Fig. 1J, K)**, although there was no significant difference in Tb.Th compared with the PTH BID group **(Fig. 1L)**. These findings indicate that PTH induces more bone volume in close and distant regions; in particular, PTH QID administration leads to the development of thicker trabeculae in regions distant from the COJ.

3.2. Distribution of ALP-positive osteoblastic cells and PHOSPHO1-reactive mature osteoblasts

The distribution of ALP-immunopositive osteoblastic cells was observed to cover all trabecular surfaces in the Sham and PTH groups **(Fig. 2A-C)**. Notably, the regions close to and distant from the COJ exhibited thicker layers of ALP-positive cells in the PTH group than in the sham group **(Fig. 2D-I)**. Statistical analysis confirmed higher ALP-positive area/TV values in the PTH groups, with the PTH QID group showing the highest ALP-positive area/TV compared with the PTH BID group in the close and distant regions **(Fig. 2J, K)**.

In contrast, in the sham group, PHOSPHO1-reactive osteoblasts accumulated primarily adjacent to the COJ **(Fig. 3A)**. The PTH BID/QID group showed numerous PHOSPHO1-reactive lines throughout the metaphyseal trabeculae **(Fig. 3B, C)**. When observed at higher magnification in the

closed region, PHOSPHO1-immunoreactive osteoblasts in the sham group were concentrated at the COJ, whereas in the PTH groups, they formed shorter lines on the trabecular bone extending from the COJ **(Fig. 3D-F)**. In the distant region, only a few PHOSPHO1-reactive short lines were observed on the trabeculae of the sham group **(Fig. 3G)**. In contrast, relatively thick and long lines of PHOSPHO1-reactive osteoblasts were observed in the PTH group **(Fig. 3H, I)**. Statistical analyses confirmed a significantly elevated PHOSPHO1-positive area/TV in the PTH groups in the close and distant regions compared to the sham group **(Fig. 3J, K)**.

3.3. Calcein labeling of trabeculae

Calcein labeling was more prominent throughout the femora in the PTH group than in the Sham group **(Fig. 4A-C)**. In the closed region, the sham group displayed relatively straight calcein labeling **(Fig. 4D)**, whereas the PTH BID/QID group exhibited fragmented and wound calcein labeling **(Fig. 4E, F)**. Conversely, in the distant region, the PTH groups showed straight and long calcein labeling compared to the sham group **(Fig. 4G-I)**. The PTH QID group displayed continuous, smooth, and longer calcein labeling than the PTH BID group **(Fig. 4H, I)**. Statistical analysis of BFR revealed a consistent increase in the PTH QID, PTH BID, and Sham groups in the regions close to and distant from the COJ **(Fig. 4J, K)**. The average length of calcein labeling was similar in the region close to the COJ, with no significant differences among the groups **(Fig. 4L)**. However, in the PTH group, it increased, with the

PTH QID group displaying the highest average length of calcein labeling in the region distant from the COJ **(Fig. 4M)**.

3.4. Distribution of TRAP-positive osteoclasts

TRAP-positive osteoclasts were primarily localized in the region close to the COJ, with fewer osteoclasts observed in the distant region in all groups **(Fig. 5A-I)**. Statistical analysis revealed an increased Oc. N/TV in the regions close to and distant from the COJ in the order of the PTH QID, PTH BID, and Sham groups **(Fig. 5J, K)**. Oc. N/BS was higher in the region close to the COJ in the PTH QID group than that in the PTH BID group **(Fig. 5L)**. However, there were no significant differences in Oc.N/BS in distant regions among all groups **(Fig. 5M)**.

3.5. Distribution of podoplanin-positive osteoblasts and osteocytes

Podoplanin-positive osteoblasts and osteocytes were abundant in the metaphyses, including in the region close to the COJ, in all groups **(Fig. 6A-F)**. However, in the distant region, the PTH groups exhibited numerous cuboidal podoplanin-positive cells, whereas the sham group showed fewer podoplanin-positive cells **(Fig. 6G-I)**. Statistical analyses confirmed a significant increase in the podoplanin-positive area/TV index in the PTH group compared to that in the sham group, with the values being lower than those in the close region, but still elevated in the distant region **(Fig. 6J, K)**. Thus, PTH administration likely facilitates osteoblast differentiation into osteocytes.

To determine whether bone-mineralizing osteoblasts could differentiate into osteocytes under normal and PTH-derived anabolic conditions, the localization of PHOSPHO1-positive osteoblasts, representing bone-mineralizing osteoblasts, and podoplanin-reactive osteoblasts to differentiate into osteocytes was examined. In the sham group, osteoblasts in the region close to the COJ tended to exhibit spatially separated podoplanin and PHOSPHO1 immunoreactivity in the Sham group **(Fig. 7A)**. In contrast, many osteoblasts in the PTH group exhibited podoplanin and PHOSPHO1 immunoreactivity **(Fig. 7B, C)**. In the trabeculae distant from the COJ, fewer osteoblasts expressed podoplanin and PHOSPHO1 in the Sham group **(Fig. 7D)**. However, in the PTH groups, particularly the PTH QID group, numerous osteoblasts exhibited co-localization of podoplanin and PHOSPHO1 **(Fig. 7E, F)**. Statistical analysis confirmed a higher ratio of osteoblasts co-localizing podoplanin and PHOSPHO1 in the close and distant regions of the COJ in the PTH group than in the sham group **(Fig. 7G, H)**.

4. Discussion

The primary objective of this study was to elucidate whether PTH administration results in remodeling- or modeling-based bone formation in different regions of the murine femora. Based on these results, we investigated whether the timing of osteoblastic differentiation into osteocytes differs in regions featuring PTH-driven remodeling or modeling-based bone formation. Our assessment yielded the

following observations:

1) In the vicinity of the COJ, the PTH QID group exhibited higher Tb.N, whereas the PTH BID group displayed significantly increased Tb.Th. In regions distant from the COJ, the PTH QID group showed higher BV/TV, Tb.N, and Tb.Th values across all groups. Consequently, it is plausible that frequent PTH administration leads to the formation of numerous fine trabeculae near the COJ and thicker trabeculae in distant regions.
2) ALP-positive osteoblasts were prevalent around most metaphyseal trabeculae close to and distant from the COJ in all groups. However, mature osteoblasts displaying PHOSPHO1-reactivity primarily formed long lines along the trabeculae distant from the COJ in the PTH groups, whereas the sham group exhibited only a few PHOSPHO1-reactive lines in distant regions.
3) BFR was markedly increased in the PTH BID group, with an even greater elevation in the PTH QID groups close to and distant from the COJ. The average calcein-labeling length was shorter in nearby regions in all groups. Consistent with the distribution of PHOSPHO1, the PTH QID group exhibited the longest average length of calcein labeling in regions distant from the COJ. Consequently, frequent PTH administration appears to accelerate bone formation in close and distant regions, with calcein labeling fragmented in the close region but continuously fragmented in the distant region.
4) Numerous TRAP-positive osteoclasts were observed in regions close to the PTH group. However, the number of osteoclasts was lower in regions distant from the COJ, with no significant differences

observed across all groups.

5) While osteoblasts in the sham group independently expressed podoplanin and PHOSPHO1 in the normal state, podoplanin and PHOSPHO1 appeared to co-localize in osteoblasts in both close and distant regions.

Taken together with the findings of PHOSPHO1, calcein labeling, and TRAP staining, it appears that frequent PTH administration primarily accelerates remodeling-based bone formation in close regions; however, modeling-based bone formation is relatively predominant in regions distant from the COJ. Therefore, distinct regions in long bones treated with PTH are likely to exhibit different patterns of bone formation. Bone-mineralizing osteoblasts seemed to facilitate differentiation into osteocytes in close and distant regions, which were relatively predominant in PTH-driven remodeling- and modeling-based bone formation, respectively.

One may wonder why different regions exhibit various PTH-driven anabolic effects. We hypothesized that, under normal conditions, numerous osteoclasts and osteoblasts actively interact to remodel the primary trabeculae composed of mineralized central cartilage cores covered with bone matrix into secondary trabeculae [29]. In contrast, recently remodeled trabeculae may not be readily resorbed. If so, it is possible that bone remodeling readily occurs in regions close to the COJ. In addition, we previously reported that the primary trabeculae close to the COJ showed less immunoreactivity for sclerostin, but relative abundance of sclerostin in the secondary trabeculae distant from the COJ [31]. Considering the basic potential of activating osteoclasts and osteoblasts, we

assumed that the region close to the COJ would possess a high potential to stimulate the coupling of osteoclasts and osteoblasts and would be more active with PTH administration. However, this was not the case in the region distant from the COJ.

Since PTH may primarily target osteoblastic cells [32], it seems reasonable that the PHOSPHO1-positive area/TV and the average length of calcein labeling would be elevated in distant regions, even without an increase in TRAP-osteoclasts. Unlike bone remodeling, modeling-based bone formation, especially minimodeling of bone trabeculae induced by the activation of osteoblasts independent of bone resorption [9, 33], reveals continuous smooth long lines in rodents and humans, respectively, when administered with eldecalcitol, an analog of the active form of vitamin D3 [10, 20] and romosozumab [12]. Therefore, the long smooth lines of calcein labeling strongly suggest that osteoblasts mineralized the bone matrix through modeling-based bone formation. In contrast, the fragmented winding lines observed in the region close to the COJ indicate remodeling-based bone formation, showing bone resorption preceding bone formation.

Taken together, these results suggest that the region distant from the COJ may have less potential to activate osteoclasts than that close to the COJ. PTH administration may preferentially accelerate remodeling-based bone formation in nearby regions, whereas model-based bone formation may often occur in regions distant from the COJ.

However, researchers believe that PTH induces remodeling rather than modeling-based bone formation [1, 2, 5]. Therefore, we assumed the limitations of using small laboratory animals, such as

mice. However, in the case of human osteoporosis, bone metabolic turnover would be elevated in postmenopausal osteoporosis, showing different bone turnover in distinct regions of the bone. It is necessary to further investigate the histological mechanism of anabolic PTH action in distinct bone regions in patients with osteoporosis.

Our subsequent inquiry centered on the ability of bone-mineralizing osteoblasts to differentiate into osteocytes, specifically within regions characterized by remodeling- and modeling-based bone formation. By concurrently detecting PHOSPHO1 and podoplanin, this study demonstrated that osteoblasts could mineralize the bone matrix and differentiate into osteocytes at different times under normal physiological conditions. PTH administration expedited the temporal progression of osteoblast differentiation into osteocytes. Consequently, osteoblasts simultaneously differentiate into osteocytes within both remodeling- and modeling-based bone formation regions, even when engaged in bone matrix mineralization. We hypothesized that the temporal dynamics of osteoblastic differentiation into osteocytes are accelerated in regions undergoing PTH-driven remodeling or modeling-based bone formation. Notably, the timing of osteoblastic differentiation into osteocytes was unaffected by remodeling- or modeling-based bone formation. We documented that immature bone that formed rapidly possessed irregularly distributed osteocytes and their cytoplasmic processes, whereas mature bone showed a regularly arranged distribution of osteocytes [31, 34-36]. The geometrical regularity of osteocyte distribution is associated with peripheral mineralization, molecular transport, and mechanical sensing [35, 37-40]. Therefore, it is necessary to investigate the geometrical regularity of

the distribution of osteocytes embedded in PTH-driven remodelling and modelling-based bone formation.

5. Conclusion

Intermittent PTH administration is likely to promote bone remodeling, ultimately resulting in remodelling-based bone formation in the metaphyseal trabeculae near the COJ of the mouse femora, whereas modelling-based bone formation is relatively predominant in regions distant from the COJ. However, it seems likely that the timing of osteoblastic differentiation into osteocytes is unaffected by the manner of remodeling- or modeling-based bone formation.

Acknowledgment

We thank Dr. Nakamura M, Dr. Yang MC, and Dr. Mayanagi M of Tohoku University for their assistance.

Ethical Approval

This study followed the principles of animal care and research set by Hokkaido University.

Funding Statement

This study was partially supported by grants from the Japan Society for the Promotion of Science (JSPS, 21H03103 to Amizuka N, 22K0991 to Hasegawa T, 23K15961 to Yokoyama A, and 23K09114 to Sekiguchi T).

Author Contributors

Hasegawa T designed the study and drafted the manuscript. Haraguchi-Kitakamae M was the first author of the original draft and the analysis and interpretation of the data. Nakajima Y, Yamamoto T, and Hongo H contributed to the immunohistochemistry. Jiaxin C, Shi Y, Liu X, Yao Q, Maroka H, Abe M, Sekiguchi T, and Yokoyama A performed bone histomorphometry and statistical analyses and critically read the manuscript. Sasano Y and Amizuka N participated in the discussion, editing, and manuscript formatting.

Conflict of interest

The authors declare no competing interests.

References

1. Lindsay R, Nieves J, Formica C, Henneman E, Woelfert L, Shen V, Dempster D, Cosman F. Randomised controlled study of effect of parathyroid hormone on vertebral-bone mass and fracture incidence among postmenopausal women on oestrogen with osteoporosis. Lancet. 1997; 350(9077):550-5.

2. Luiz de Freitas PH, Li M, Ninomiya T, Nakamura M, Ubaidus S, Oda K, Udagawa N, Maeda T, Takagi R, Amizuka N. Intermittent PTH administration stimulates pre-osteoblastic proliferation without leading to enhanced bone formation in osteoclast-less c-fos(-/-) mice. J Bone Miner Res. 2009;24(9):1586-97.

3. Zhao S, Hasegawa T, Hongo H, Yamamoto T, Abe M, Yoshida T, Haraguchi M, de Freitas PHL, Li M, Tei K, Amizuka N.Intermittent PTH Administration Increases Bone-Specific Blood Vessels and Surrounding Stromal Cells in Murine Long Bones. Calcif Tissue Int. 2021;108(3):391-406.

4. Yamamoto T, Maruoka H, Hongo H, Yoshino H, Haraguchi-Kitakamae M, Liu X, Yao Q, Li M, Amizuka N, Hasegawa T. Early gene expression profiles of anabolic and catabolic molecules in murine bone after a single PTH injection. J Oral Biosci. 2023;65(4):395-400.

5. Serge L. Ferrari. Romosozumab to rebuild the foundations of bone strength. Nature Reviews Rheumatology. 2018;14(3):128.

6. Pazianas M. Anabolic effects of PTH and the 'anabolic window' Trends Endocrinol Metab. 2015;26(3):111-3.

7. Frost HM. Mechanical determinants of bone modeling Metab Bone Dis Relat Res. 1982;4(4):217-29.

8. Erben RG. Trabecular and endocortical bone surfaces in the rat: modeling or remodeling? Anat Rec. 1996; 246(1):39-46.

9. Jee WS, Tian XY and Setterberg RB. Cancellous bone minimodeling-based formation: a Frost, Takahashi legacy. J Musculoskelet Neuronal Interact 2007;7(3):232-9.

10. Hasegawa T, Yamamoto T, Sakai S, Miyamoto Y, Hongo H, Qiu Z, Abe M, Takeda S, Oda K, de Freitas PHL, Li M, Endo K, Amizuka N. Histological Effects of the Combined Administration of Eldecalcitol and a Parathyroid Hormone in the Metaphyseal Trabeculae of Ovariectomized Rats. J Histochem Cytochem. 2019;67(3):169-184.

11. Cosman F, Crittenden DB, Adachi JD, Binkley N, Czerwinski E, Ferrari S, Hofbauer LC, Lau E, Lewiecki EM, Miyauchi A, Zerbini CA, Milmont CE, Chen L, Maddox J, Meisner PD, Libanati C, Grauer A. Romosozumab Treatment in Postmenopausal Women with Osteoporosis. N Engl J Med. 2016; 375(16):1532-1543.

12. Chavassieux P, Chapurlat R, Portero-Muzy N, Roux JP, Garcia P, Brown JP, Libanati C, Boyce RW, Wang A, Grauer A. Bone-Forming and antiresorptive effects of romosozumab in postmenopausal women with osteoporosis: Bone histomorphometry and microcomputed tomography analysis after 2 and 12 months of treatment. J Bone Miner Res. 2019;34(9):1597-1608.

13. Ominsky MS, Brown DL, Van G, Cordover D, Pacheco E, Frazier E, Cherepow L, Higgins-Garn M, Aguirre JI, Wronski TJ, Stolina M, Zhou L, Pyrah I, Boyce RW. Differential temporal effects of sclerostin antibody and parathyroid hormone on cancellous and cortical bone and quantitative differences in effects on the osteoblast lineage in young intact rats. Bone. 2015;81:380-391.

14. Yamamoto T, Hasegawa T, Sasaki M, Hongo H, Tsuboi K, Shimizu T, Ota M, Haraguchi M, Takahata M, Oda K, Luiz de Freitas PH, Takakura A, Takao-Kawabata R, Isogai Y, Amizuka N.

Frequency of teriparatide administration affects the histological pattern of bone formation in young adult male mice. Endocrinology. 2016;157(7):2604-20.

15. Mae T, Hasegawa T, Hongo H, Yamamoto T, Zhao S, Li M, Yamazaki Y, Amizuka N. Immunolocalization of enzymes/membrane transporters related to bone mineralization in the metaphyses of the long bones of parathyroid-hormone-administered aice. Medicina (Kaunas). 2023;59(6):1179.

16. Oda K, Amaya Y, Fukushi-Irie M, Kinameri Y, Ohsuye K, Kubota I, Fujimura S, Kobayashi J. A general method for rapid purification of soluble versions of glycosylphosphatidylinositol-anchored proteins expressed in insect cells: An application for human tissue-nonspecific alkaline phosphatase. J. Biochem. 1999;126:694–699.

17. Hasegawa T. Ultrastructure and biological function of matrix vesicles in bone mineralization. Histochem Cell Biol. 2018;149(4):289-304.

18. Roberts SJ, Stewart AJ, Sadler PJ, Farquharson C. Human PHOSPHO1 exhibits high specific phosphoethanolamine and phosphocholine phosphatase activities. Biochem. J. 2004;82:59–65.

19. Roberts S, Narisawa S, Harmey D, Millán J.L, Farquharson C. Functional involvement of PHOSPHO1 in matrix vesicle-mediated skeletal mineralization. J. Bone Miner. Res. 2007;22:617–627.

20. Hasegawa T, Yamamoto T, Sakai S, Miyamoto Y, Hongo H, Qiu Z, Abe M, Takeda S, Oda K, de Freitas PHL, Li M, Endo K, Amizuka N. Histological Effects of the Combined Administration of Eldecalcitol and a Parathyroid Hormone in the Metaphyseal Trabeculae of Ovariectomized Rats. J Histochem Cytochem. 2019;67(3):169-184.

21. Breiteneder-Geleff S, Matsui K, Soleiman A, Meraner P, Poczewski H, Kalt R, Schaffner G, Kerjaschki D. Podoplanin, novel 43-kd membrane protein of glomerular epithelial cells, is down-regulated in puromycin nephrosis. Am J Pathol. 1997;151(4):1141-52.

22. Wetterwald A, Hoffstetter W, Cecchini MG, Lanske B, Wagner C, Fleisch H, Atkinson M. Characterization and cloning of the E11 antigen, a marker expressed by rat osteoblasts and osteocytes. Bone. 1996;18(2):125-32.

23. Barragan-Adjemian C, Nicolella D, Dusevich V, Dallas MR, Eick JD, Bonewald LF. Mechanism by which MLO-A5 late osteoblasts/early osteocytes mineralize in culture: similarities with

mineralization of lamellar bone. Calcif Tissue Int. 2006;79(5):340-53.

24. Nefussi JR, Sautier JM, Nicolas V, Forest N. How osteoblasts become osteocytes: a decreasing matrix forming process. J BiolBuccale. 1991;19(1):75-82.

25. Zhang K, Barragan-Adjemian C, Ye L, Kotha S, Dallas M, Lu Y, Zhao S, Harris M, Harris SE, Feng JQ, Bonewald LF. E11/gp38 selective expression in osteocytes: regulation by mechanical strain and role in dendrite elongation. Mol Cell Biol. 2006;26(12):4539-52.

26. Nagai T, Hasegawa T, Yimin, Yamamoto T, Hongo H, Abe M, Yoshida T, Yokoyama A, de Freitas PHL, Li M, Yokoyama A, Amizuka N. Immunocytochemical assessment of cell differentiation of podoplanin-positive osteoblasts into osteocytes in murine bone. Histochem Cell Biol. 2021;155(3):369-380.

27. Hasegawa T, Tokunaga S, Yamamoto T, Sakai M, Hongo H, Kawata T, Amizuka N. Evocalcet Rescues Secondary Hyperparathyroidism-driven Cortical Porosity in CKD Male Rats. Endocrinology. 2023;11;164(4):bqad022.

28. Muneyama T, Hasegawa T, Yimin, Yamamoto T, Hongo H, Haraguchi-Kitakamae M, Abe M,

Maruoka H, Ishizu H, Shimizu T, Sasano Y, Li M, Amizuka N. Histochemical assessment on osteoclasts in long bones of toll-like receptor 2 (TLR2) deficient mice. J Oral Biosci. 2023;65(2):163-174.

29. Parfitt AM, Drezner MK, Glorieux FH, Kanis JA, Malluche H, Meunier PJ, Ott SM, Recker RR. Bone histomorphometry: standardization of nomenclature, symbols, and units. Report of the ASBMR Histomorphometry Nomenclature Committee. J Bone Miner Res. 1987;2(6):595-610.

30. Amizuka N, Hasegawa T, Oda K, Luiz de Freitas PH, Hoshi K, Li M, Ozawa H. Histology of epiphyseal cartilage calcification and endochondral ossification. Front Biosci (Elite Ed). 2012;1;4(6):2085-100.

31. Hasegawa T, Amizuka N, Yamada T, Liu Z, Miyamoto Y, Yamamoto T, Sasaki M, Hongo H, Suzuki R, de Freitas PH, Yamamoto T, Oda K, Li M. Sclerostin is differently immunolocalized in metaphyseal trabecules and cortical bones of mouse tibiae. Biomed Res. 2013;34(3):153-9.

32. Amizuka N, Karaplis AC, Henderson JE, Warshawsky H, Lipman ML, Matsuki Y, Ejiri S, Tanaka M, Izumi N, Ozawa H, Goltzman D. Haploinsufficiency of parathyroid hormone-related peptide (PTHrP) results in abnormal postnatal bone development. Dev Biol. 1996;10;175(1):166-76.

33. Yamamoto T, Hasegawa T, Fraitas PHL, Hongo H, Zhao S, Yamamoto T, Nasoori A, Abe M, Maruoka H, Kubota K, Morimoto Y, Haraguchi M, Shimizu T, Takahata M, Iwasaki N, Li M, Amizuka N. Histochemical characteristics on minimodeling-based bone formation induced by anabolic drugs for osteoporotic treatment. Biomed Res. 2021;42(5):161-171.

34. Ubaidus S, Li M, Sultana S, de Freitas PH, Oda K, Maeda T, Takagi R, Amizuka N. FGF23 is mainly synthesized by osteocytes in the regularly distributed osteocytic lacunar canalicular system established after physiological bone remodeling. J Electron Microsc (Tokyo). 2009;58(6):381-92.

35. Sasaki M, Hasegawa T, Yamada T, Hongo H, de Freitas PH, Suzuki R, Yamamoto T, Tabata C, Toyosawa S, Yamamoto T, Oda K, Li M, Inoue N, Amizuka N. Altered distribution of bone matrix proteins and defective bone mineralization in klotho-deficient mice. Bone. 2013;57(1):206-19.

36. Hasegawa T, Yamamoto T, Hongo H, Qiu Z, Abe M, Kanesaki T, Tanaka K, Endo T, de Freitas PHL, Li M, Amizuka N. Three-dimensional ultrastructure of osteocytes assessed by focused ion beam-scanning electron microscopy (FIB-SEM). Histochem Cell Biol. 2018;149(4):423-432.

37. Hongo H, Hasegawa T, Saito M, Tsuboi K, Yamamoto T, Sasaki M, Abe M, Henrique Luiz de

Freitas P, Yurimoto H, Udagawa N, Li M, Amizuka N. Osteocytic osteolysis in PTH-treated wild-type and *Rankl*$^{-/-}$ mice examined by transmission electron microscopy, atomic force microscopy, and isotope microscopy. J Histochem Cytochem. 2020;68(10):651-668.

38. Qin L, Liu W, Cao H, Xiao G. Molecular mechanosensors in osteocytes. Bone Res. 2020;8;8:23.

39. Yamamoto T, Hasegawa T, Mae T, Hongo H, Yamamoto T, Abe M, Nasoori A, Morimoto Y, Maruoka H, Kubota K, Haraguchi M, Li M. Comparative immunolocalization of tissue nonspecific alkaline phosphatase and ectonucleotide pyrophosphatase/phosphodiesterase 1 in murine bone. J Oral Biosci. 2021;63(3):259-264.

40. Hasegawa T, Hongo H, Yamamoto T, Abe M, Yoshino H, Haraguchi-Kitakamae M, Ishizu H, Shimizu T, Iwasaki N, Amizuka N. Matrix vesicle-mediated mineralization and osteocytic regulation of bone mineralization. Int J Mol Sci. 2022;23(17):9941.

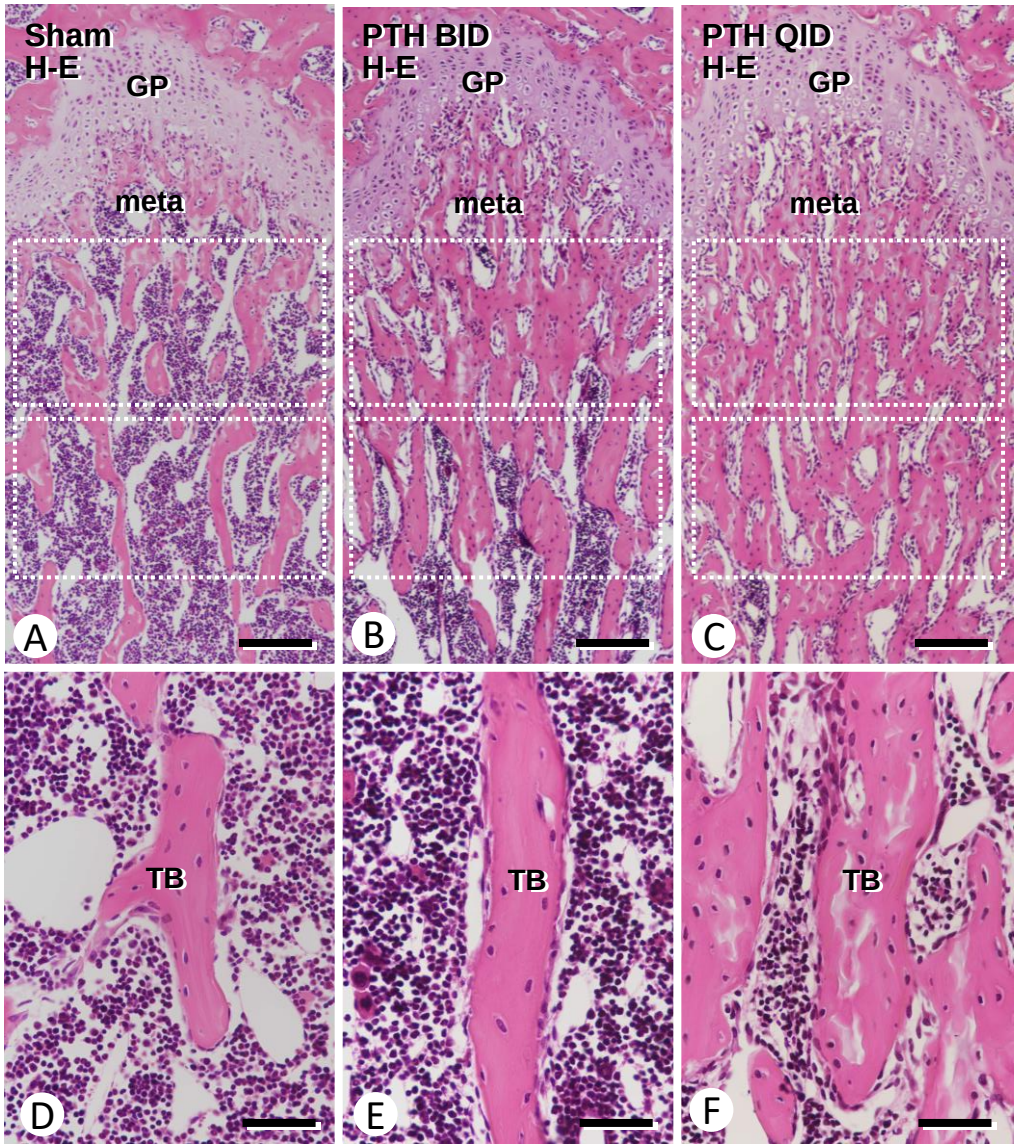
Sham
H-E
GP
meta
A
PTH BID
H-E
GP
meta
B
PTH QID
H-E
GP
meta
C
TB
D
TB
E
TB
F

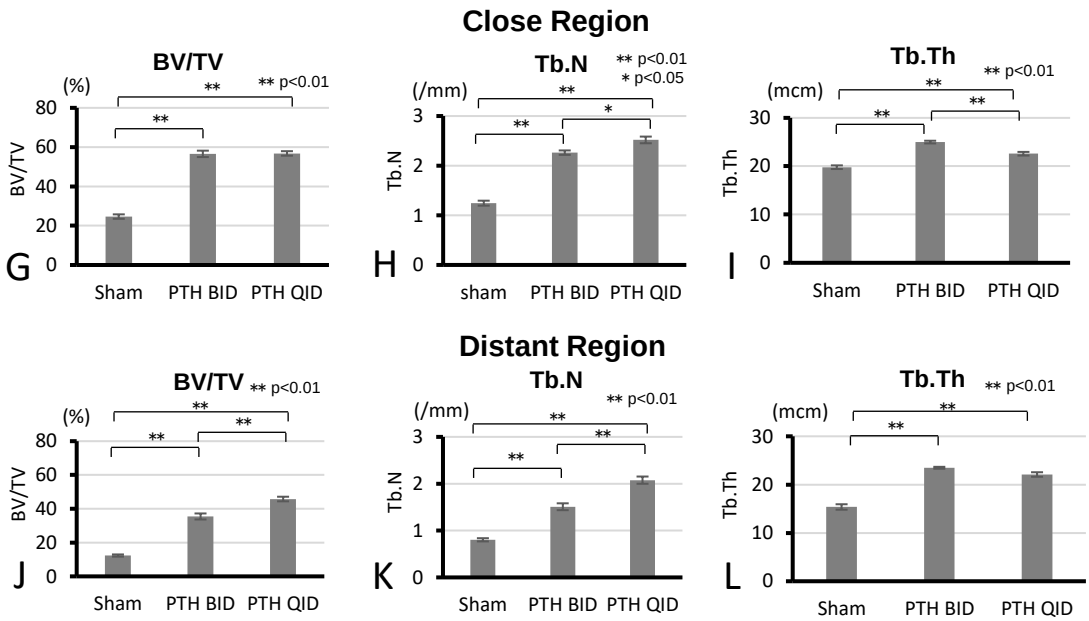
Close Region
BV/TV
(%)
** p<0.01
BV/TV
80
60
40
20
0
Sham
PTH BID
PTH QID
G
Tb.N
** p<0.01
* p<0.05
(/mm)
Tb.N
3
2
1
0
sham
PTH BID
PTH QID
H
Tb.Th
** p<0.01
(mcm)
Tb.Th
30
20
10
0
Sham
PTH BID
PTH QID
I
Distant Region
BV/TV
** p<0.01
(%)
BV/TV
80
60
40
20
0
Sham
PTH BID
PTH QID
J
Tb.N
** p<0.01
(/mm)
Tb.N
3
2
1
0
Sham
PTH BID
PTH QID
K
Tb.Th
** p<0.01
(mcm)
Tb.Th
30
20
10
0
Sham
PTH BID
PTH QID
L

Fig.1

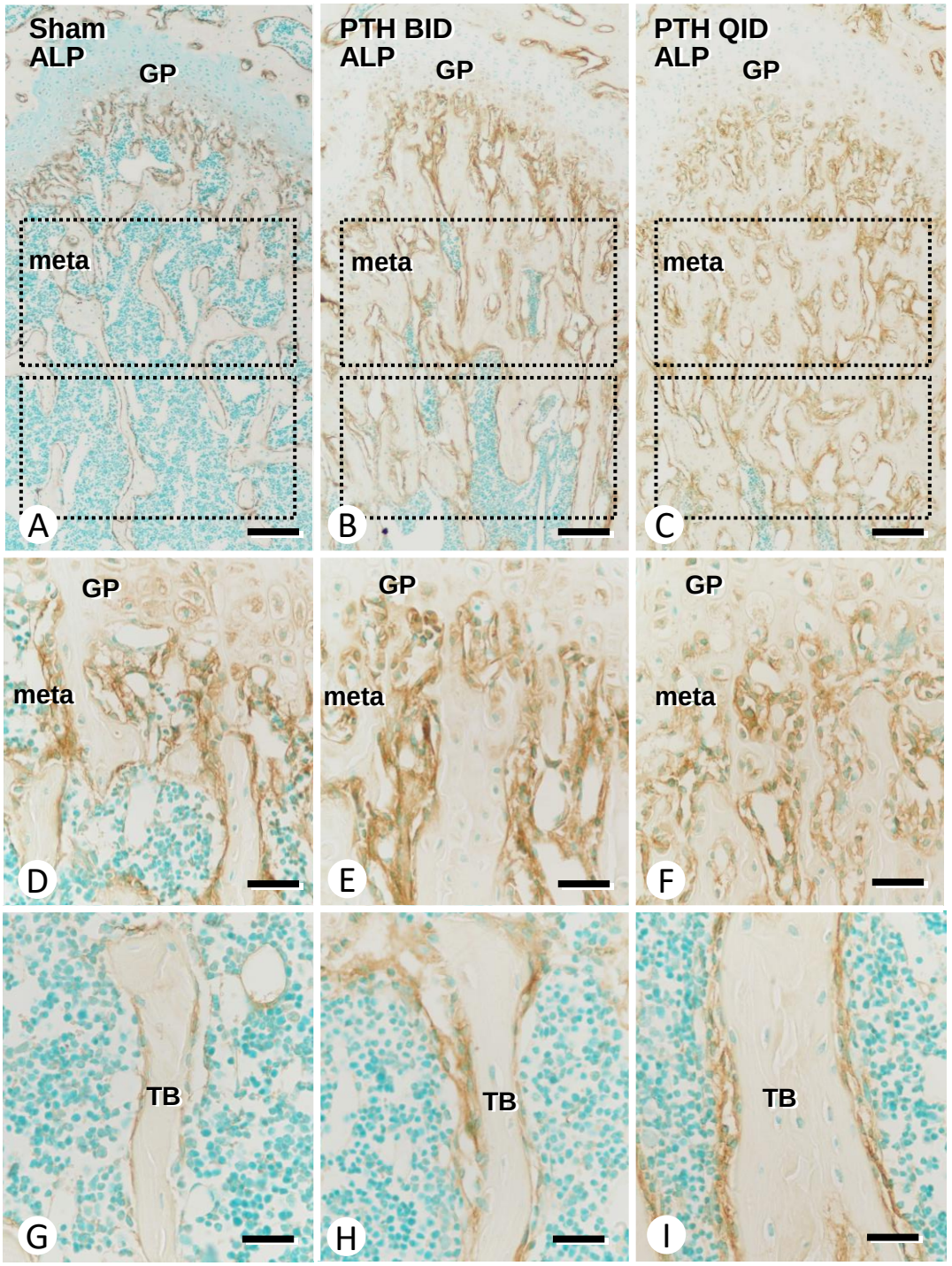
Sham
ALP
GP
meta
A
PTH BID
ALP
GP
meta
B
PTH QID
ALP
GP
meta
C
GP
meta
D
GP
meta
E
GP
meta
F
TB
G
TB
H
TB
I

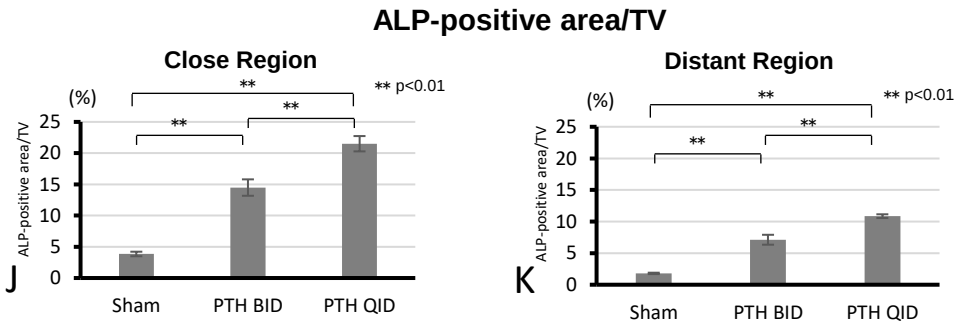
ALP-positive area/TV
Close Region
(%)
** p<0.01
ALP-positive area/TV
25
20
15
10
5
0
Sham
PTH BID
PTH QID
J
Distant Region
(%)
** p<0.01
ALP-positive area/TV
25
20
15
10
5
0
Sham
PTH BID
PTH QID
K

Fig.2

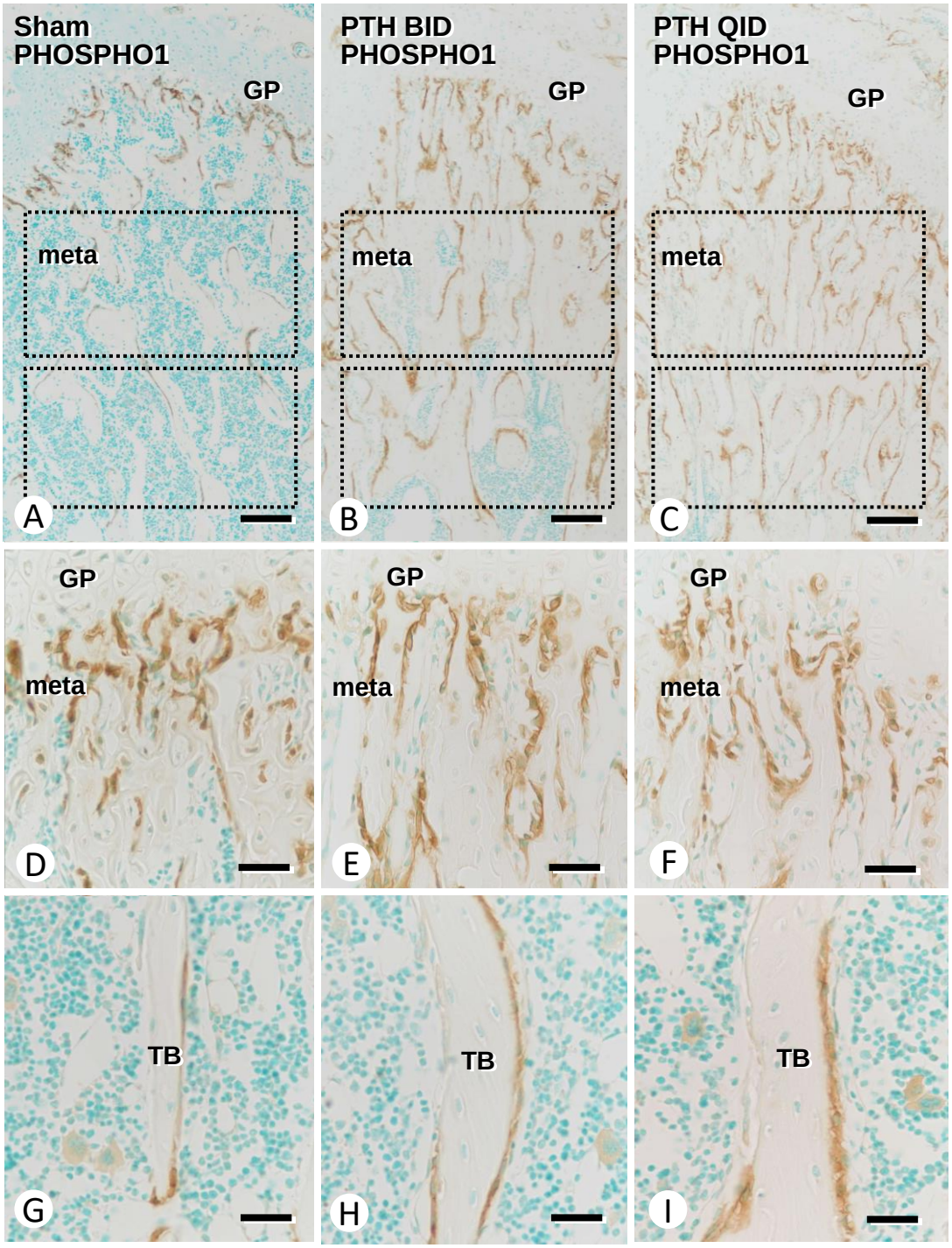
Sham
PHOSPHO1
PTH BID
PHOSPHO1
PTH QID
PHOSPHO1
GP
meta
TB
A
B
C
D
E
F
G
H
I

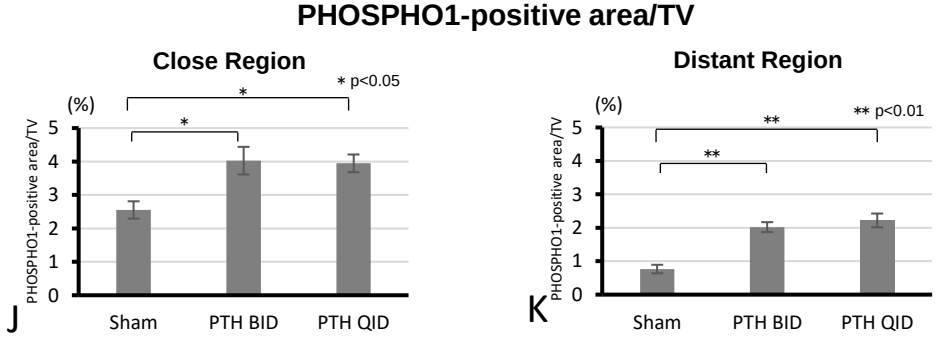
PHOSPHO1-positive area/TV
Close Region
Distant Region
(%)
* p<0.05
** p<0.01
PHOSPHO1-positive area/TV
Sham
PTH BID
PTH QID
J
K

Fig.3

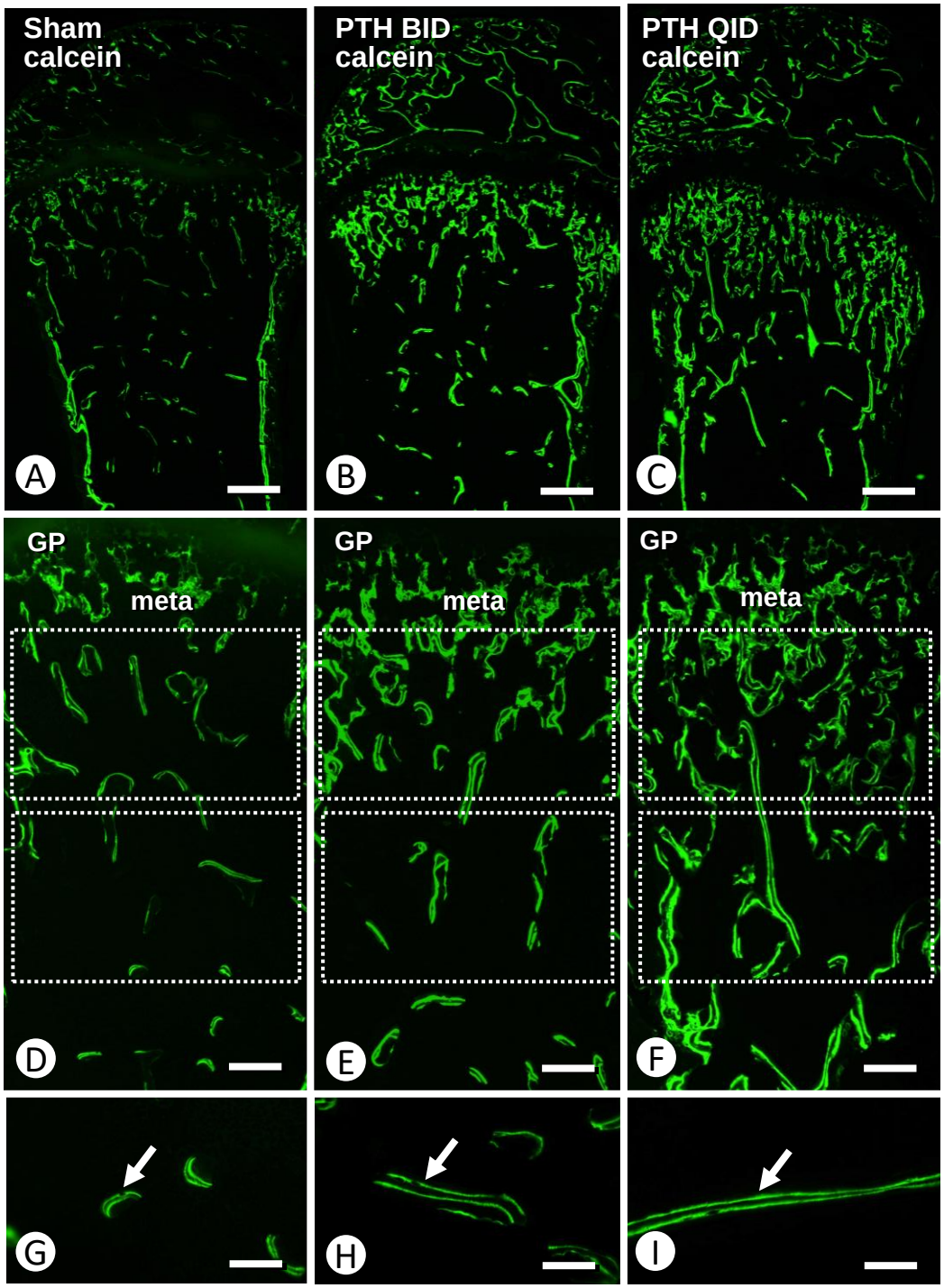
Sham calcein
PTH BID calcein
PTH QID calcein
A
B
C
GP
meta
D
E
F
G
H
I

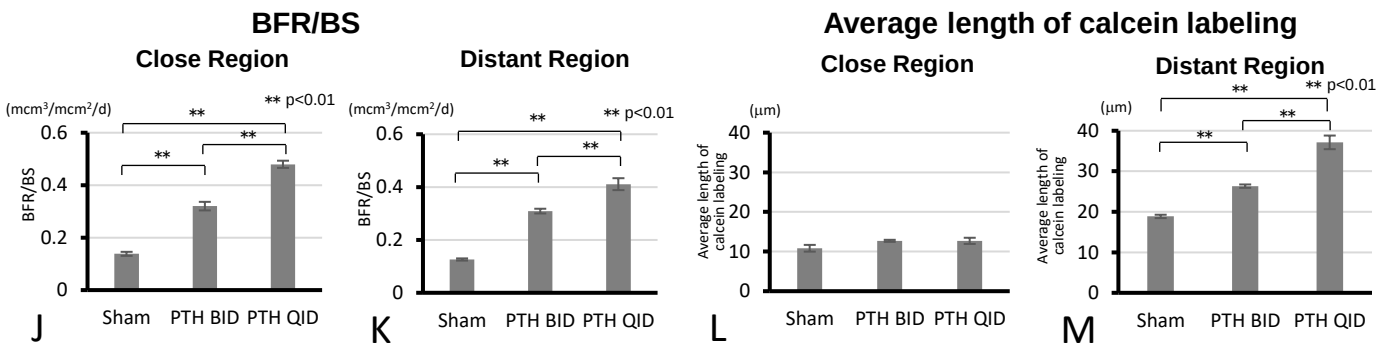
BFR/BS
Close Region
Distant Region
(mcm³/mcm²/d)
** p<0.01
BFR/BS
0.6
0.4
0.2
0
Sham
PTH BID
PTH QID
J
K
Average length of calcein labeling
Close Region
Distant Region
(μm)
Average length of calcein labeling
40
30
20
10
0
L
M

Fig.4

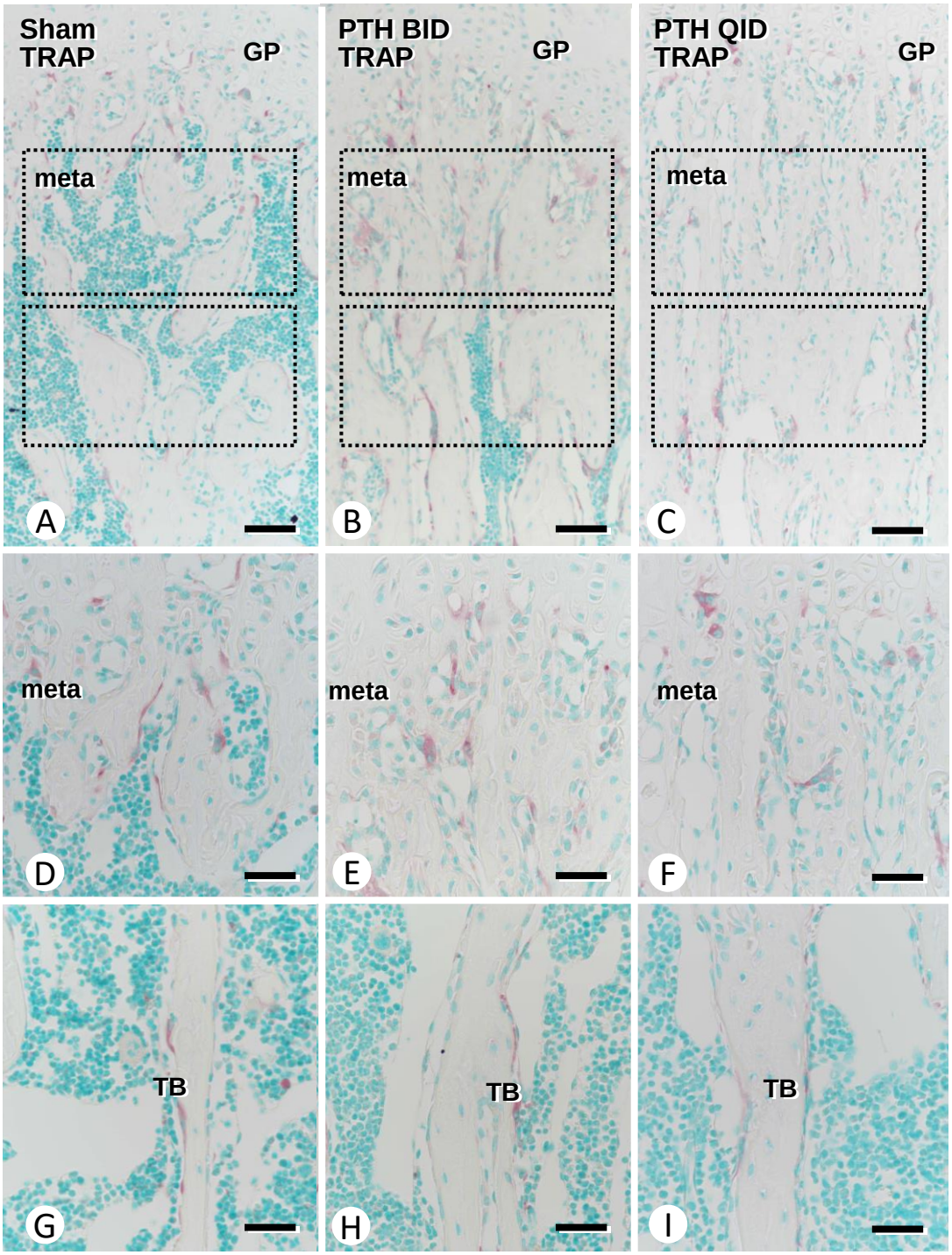
Sham
TRAP
GP
meta
A
PTH BID
TRAP
GP
meta
B
PTH QID
TRAP
GP
meta
C
meta
D
meta
E
meta
F
TB
G
TB
H
TB
I

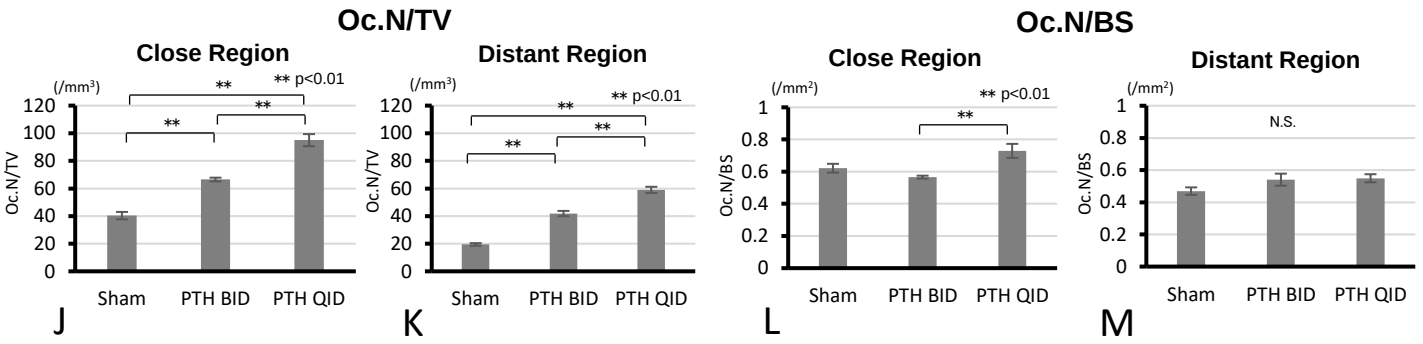
Oc.N/TV
Close Region
(/mm³)
** p<0.01
**
**
**
120
100
80
60
40
20
0
Oc.N/TV
Sham
PTH BID
PTH QID
J
Distant Region
(/mm³)
** p<0.01
**
**
**
120
100
80
60
40
20
0
Oc.N/TV
Sham
PTH BID
PTH QID
K
Oc.N/BS
Close Region
(/mm²)
** p<0.01
**
1
0.8
0.6
0.4
0.2
0
Oc.N/BS
Sham
PTH BID
PTH QID
L
Distant Region
(/mm²)
N.S.
1
0.8
0.6
0.4
0.2
0
Oc.N/BS
Sham
PTH BID
PTH QID
M

Fig.5

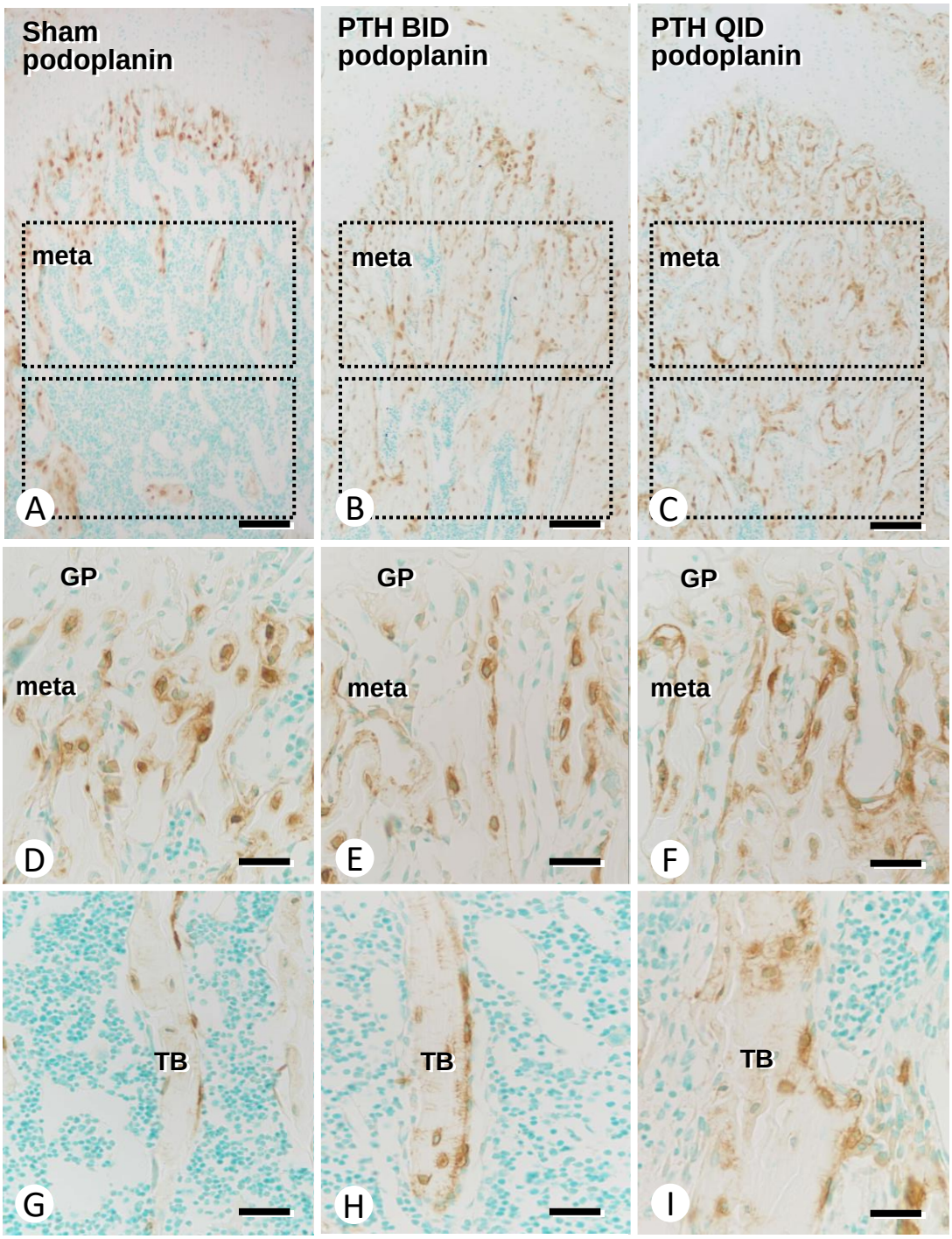
Sham
podoplanin
PTH BID
podoplanin
PTH QID
podoplanin
meta
meta
meta
A
B
C
GP
GP
GP
meta
meta
meta
D
E
F
TB
TB
TB
G
H
I

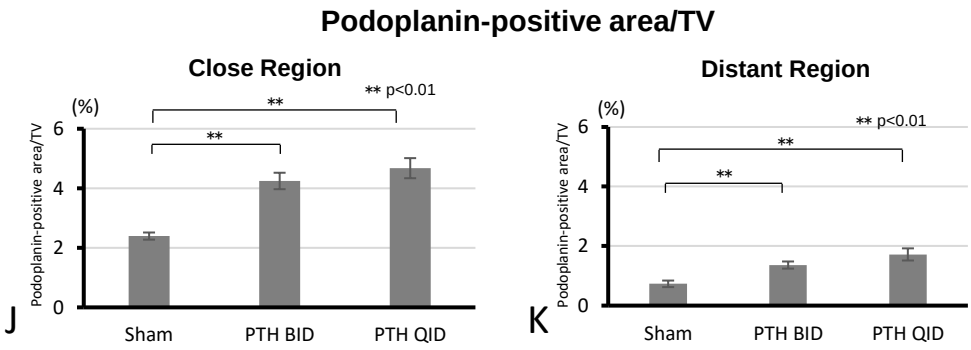
Podoplanin-positive area/TV
Close Region
Distant Region
(%)
Podoplanin-positive area/TV
** p<0.01
**
**
0
2
4
6
Sham
PTH BID
PTH QID
J
K

Fig.6

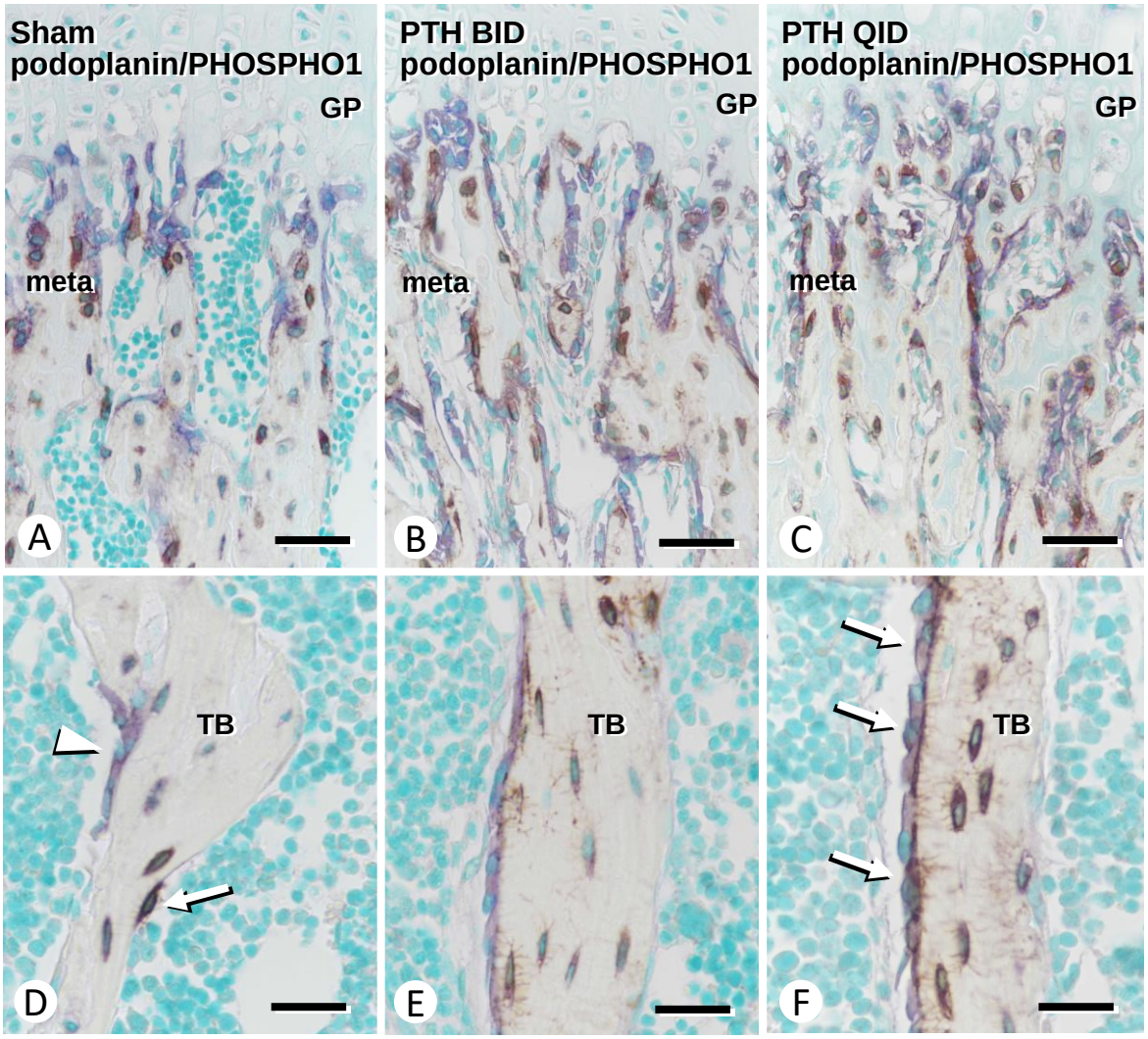
Sham
podoplanin/PHOSPHO1
GP
meta
A
PTH BID
podoplanin/PHOSPHO1
GP
meta
B
PTH QID
podoplanin/PHOSPHO1
GP
meta
C
TB
D
TB
E
TB
F

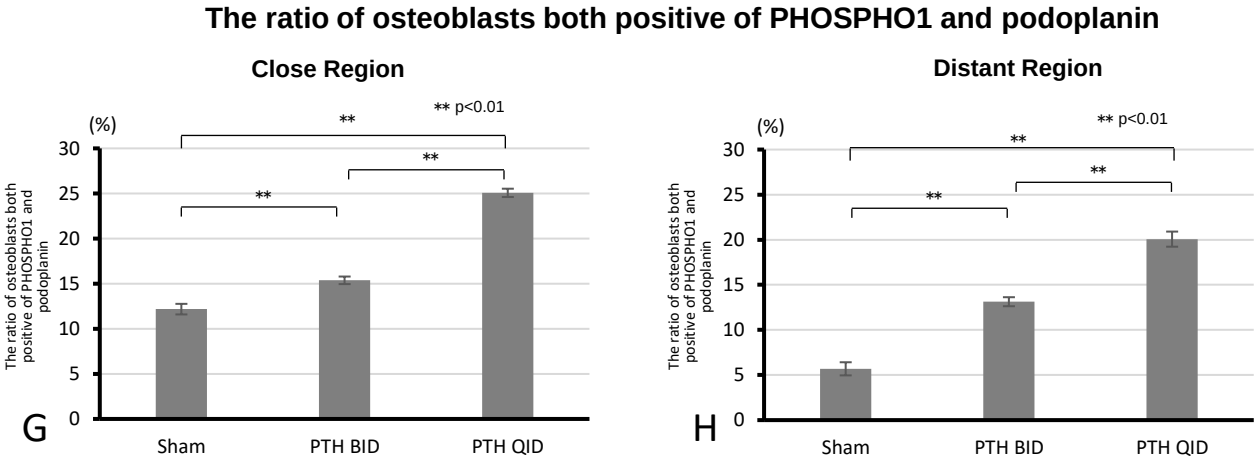
The ratio of osteoblasts both positive of PHOSPHO1 and podoplanin
Close Region
(%)
** p<0.01
**
**
**
The ratio of osteoblasts both positive of PHOSPHO1 and podoplanin
30
25
20
15
10
5
0
Sham
PTH BID
PTH QID
G
Distant Region
(%)
** p<0.01
**
**
**
The ratio of osteoblasts both positive of PHOSPHO1 and podoplanin
30
25
20
15
10
5
0
Sham
PTH BID
PTH QID
H

Fig.7

Figure legends

Figure 1

Histology of the metaphyseal trabeculae close to COJ and those distant from the COJ in mice administered with PTH

Panels A-B show low-magnification images of the femoral metaphyses (meta) of sham (A), PTH BID (B), and PTH QID (C) mice. The dotted lines represent two ROIs: the regions close to and distant from the COJ, respectively. Panels D-F show the trabeculae (TB) in the distal regions of the sham (D), PTH BID (E), and PTH QID (F) groups. Note the thick trabeculae in the PTH-treated groups (E, F compared to D). Graphs G-L show statistical analyses of the values of BV/TV (G, J), Tb.N (H, K), and Tb.Th (I, L). Panels G-I are derived from close regions, whereas panels J-L are obtained from distant regions. GP, growth plate

Bars, A-C: 300 μm, D-F: 100 μm

Figure 2

The distribution of ALP-positive osteoblastic cells in the regions close to and distant from the COJ

Panels A-C show ALP immunolocalization (brown) in the metaphyses (meta) of the sham (A), PTH BID (B), and PTH QID (C) groups. The dotted lines represent two ROIs: the regions close to and distant from the COJ, respectively. Panels D-F and G-I show highly magnified trabeculae (TB) in close

and distant regions, respectively. The lower panels (J, K) show the statistical analyses of the ALP-positive area/TV in the close (J) and distant (K) regions. GP, growth plate

Bars, A-C: 300 μm, D-I: 100 μm

Figure 3

The distribution of PHOSPHO1-reactive mature osteoblasts in the regions close to and distant from the COJ

Panels A-C show the immunolocalization of PHOSPHO1 (brown) in the metaphyses (meta) of the sham (A), PTH BID (B), and PTH QID (C) groups. The dotted lines represent two ROIs: the regions close to and distant from the COJ, respectively. Panels D-F display highly magnified images of the distribution of PHOSPHO1-reactive osteoblasts. PHOSPHO1-reactive osteoblasts accumulated beneath the growth plate (GP) in the region close to the sham group (D), while PHOSPHO1-reactive osteoblasts formed lines on the trabeculae extending the growth plate in the PTH-administered groups (E, F). In the distant region, the sham group showed short lines of PHOSPHO1-reactive osteoblasts (G), whereas the PTH-treated groups demonstrated long lines of PHOSPHO1-reactive osteoblasts (H, I). The lower panels (J, K) represent statistical analyses of the PHOSPHO1-positive area/TV in the close (J) and distant (K) regions.

Bars, A-C: 300 μm, D-I: 100 μm

Figure 4

Calcein labeling in the trabeculae close to and distant from the COJ

Panels A-C and D-F demonstrate calcein labeling (green color) in the distal region of the femora and metaphyses (meta) of the sham (A, D), PTH BID (B, E), and PTH QID (C, F) groups, respectively. The dotted lines represent two ROIs: the regions close to and distant from the COJ, respectively. Panels G-I show highly magnified images of calcein labeling of the trabeculae in the distal regions of the sham (G), PTH BID (H), and PTH QID (I) groups. Note the many fine curly calcein labels in the region close to the COJ in the PTH-administered groups (E, F) when compared to the sham group (D). Panels F and I clearly show long continuous lines of calcein labeling in the region distant from the PTH QID group (arrows in G-I). The lower panels represent statistical analyses of the bone formation rate and average length of calcein labeling (J-M). In regions close to and distant from the COJ, the bone formation rate was higher in the PTH QID, PTH BID, and Sham groups (J, K). There was no significant difference in the average length of calcein labeling in the closed region (L); however, it was increased in the PTH group (M). Note the longer calcein line in PTH-QID group. GP, Growth plate

Bars, A-C: 600 μm, D-F: 200 μm, G-I: 100 μm

Figure 5

The distribution of TRAP-positive osteoclasts in the trabeculae close to and distant from the COJ

Panels A-C show the distribution of TRAP-positive osteoclasts (red) in the femoral metaphyses (meta) of the sham (A), PTH BID (B), and PTH QID (C) groups. The dotted lines represent two ROIs: the regions close to and distant from the COJ, respectively. Panels D-F and G-I display highly magnified images of the localization of TRAP-positive osteoclasts in the closed region (D-F) and the distal regions (G-I) of the Sham (D, G), PTH BID (E, H), and PTH QID (F, I) groups. The lower panels represent the statistical analyses of Oc. N/TV and Oc. N/BS (J-M). The PTH-administered groups showed an increase in Oc.N/TV in the close and distant regions compared to the sham groups (J, K). The PTH QID group showed a significant increase in Oc.N/BS in the close region compared to the Sham and PTH BID groups (L). However, there was no significant difference in the value of Oc. N/BS in distant regions among all groups (M). GP, Growth plate; TB, trabecula

Bars, A-C: 200 μm, D- I: 100 μm

Figure 6

The distribution of podoplanin-positive osteoblasts and osteocytes in the regions close to and distant from the COJ

Panels A-C show the distribution of podoplanin-positive osteoblasts/osteocytes (brown) in the femoral metaphyses (meta) of the sham (A), PTH BID (B), and PTH QID (C) groups. The dotted lines represent two ROIs: the regions close to and distant from the COJ, respectively. Panels D-F and G-I show highly magnified images of the distribution of podoplanin-positive osteoblasts/osteocytes in the close (D-F)

and distal (G-I) regions of the sham (D, G), PTH BID (E, H), and PTH QID (F, I) groups. Statistical analyses showed a significant increase in the podoplanin-positive area/TV index in the PTH group compared to that in the sham group (J, K). GP, Growth plate; TB, trabecula

Bars, A-C: 300 μm, D- I: 50 μm

Figure 7

The distribution of podoplanin/PHOSPHO1-positive osteoblasts in the regions close to and distant from the COJ

Panels A-C and D-F demonstrate the double detection of PHOSPHO1-positive (blue) and podoplanin-reactive (brown) osteoblasts/osteocytes in the trabeculae of close and distant regions, respectively. Osteoblasts bearing podoplanin (arrow in D) and PHOSPHO1-positive osteoblasts (arrowhead in D) were localized separately. In contrast, many osteoblasts in the PTH QID group expressed both podoplanin and PHOSPHO1 (arrows in F). Statistical analysis demonstrated a higher ratio of osteoblasts merging the immunoreactivity of podoplanin and PHOSPHO1 in the close (G) and distant (H) regions of the PTH group than in the sham group.

Bars, A-C: 100 μm, D-F: 50 μm

primary antibody	cat. No.	company	dilution
Rabbit polyclonal antisera against TNALPase		Provided by Dr. Oda [16]	1: 300
Rabbit polyclonal anti-PHOSPHI1	Q8TCT1	Cusabio Technology Llc., Houston, TX	1: 100
Goat polyclonal anti-podoplanin	AF3244	R&D systems, Inc., Minneapolis, MN	1: 100

secondary antibody	cat. No.	company	dilution
HRP-conjugated anti-rabbit IgG	P0399	DakoCytomation, Glostrup, Denmark	1: 100
HRP-conjugated anti-goat IgG	A201PS	American Qualex Scientific Products, Inc., San Clemente, CA	1: 100
ALP-conjugated goat Anti-Rabbit IgG	111-055-003	Jackson ImmunoResearch Laboratories, Inc., West Grove, PA	1: 100

Supplementary table.1